RSC Advances

ROYAL SOCIETY OF CHEMISTRY

www.rsc.org/advances

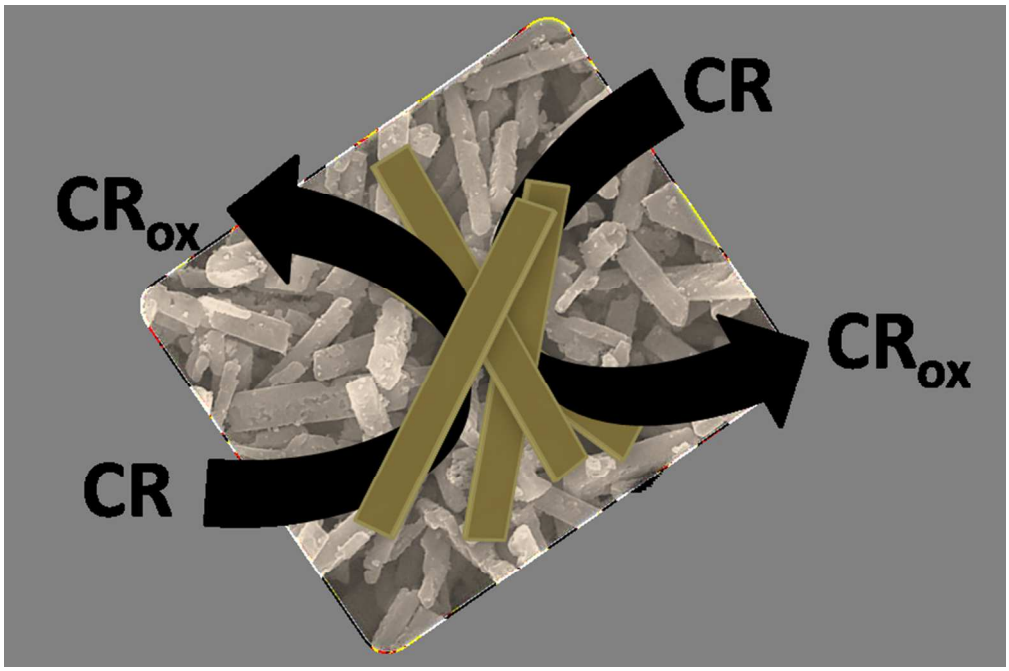

151x99mm (150 x 150 DPI)

Inorganic Chemistry FRONTIERS RSCPublishing

RESEARCH ARTICLE

Ionic liquid mediated synthesis of nitrogen, carbon and fluorine-codoped rutile TiO_2 nanorods for improved UV and visible light photocatalysis

Cite this: DOI: 10.1039/xoxxoooooox

Received ooth January 2012,
Accepted ooth January 2012

DOI: 10.1039/xoxxoooooox

www.rsc.org/

Rajesh Ramanathan[a] and Vipul Bansal[a,]*

The application of 1-butyl-3-methylimidazolium tetrafluoroborate ([BMIM][BF_4]) ionic liquid (IL) as a designer solvent for the synthesis of multiple nonmetal (N, C and F) codoped rutile titania (TiO_2) nanorods is presented. The incorporation of multiple nonmetals within the TiO_2 lattice was achieved by controlled heating of a semi-crystalline organic-inorganic complex formed via ammonia-driven hydrolysis of a titanium precursor in [BMIM][BF_4]. These multiple nonmetal codoped rutile NCF-TiO_2 nanorods showed a remarkable improvement in UV and visible light photocatalysis performance over commercial nanoparticulate Degussa P25 anatase TiO_2.

Ionic liquids (ILs) have emerged as a promising class of environmentally benign 'green' solvents because of their unique physicochemical properties such as high ionic conductivity and thermal stability as well as negligible volatility.[1,2] Such interesting properties have now allowed ILs to be regularly employed as preferred reaction media for applications in organic chemistry, biochemistry, electrochemistry and polymer chemistry.[3-5] In addition, the ability of ILs in significantly influencing the physicochemical environment of a reaction has led to facile self-assembly of biomolecules to form organic-inorganic hybrid nanomaterials.[6, 7] Given the gaining importance of ILs, it is unsurprising that fabrication of a range of inorganic oxides such as silica, titania and iron oxide as well as metal-organic semiconductors is regularly achieved in different ILs.[6-9]

Of the different transition-metal oxides, nanostructured titanium dioxide (TiO_2) has gained particular attraction as a wide band gap semiconductor due to its wide-spread use as a photocatalyst for degradation of organic dyes and pollutants.[10-12] It is well-established that the photocatalytic activity of TiO_2 is largely dependent on its phase composition,[10,13-15] wherein rutile phase is typically observed to show poorer performance over brookite and anatase phases.[16-18] While both anatase and rutile TiO_2 have been extensively studied for photocatalysis, their photoactivity has been largely restricted in response to ultraviolet (UV) excitation.[10,13-15] Since UV irradiation accounts for a minuscule (~3%) proportion of the solar energy spectrum reaching the surface of our planet, this does not allow TiO_2 to act as an outstanding photocatalyst under solar light. In contrast, earth's atmospheric opacity allows visible light to cover ~44% of the overall solar electromagnetic spectrum reaching to the earth's surface. Therefore, to improve the photoactivity of TiO_2 nanoparticles in the visible region, several strategies, particularly those focussed on reducing the band gap of TiO_2, have been employed. The two major strategies include either decoration of TiO_2 surface with metal nanoclusters[19-25] or doping TiO_2 lattice with either a transition metal or a nonmetal.[10,26-28] Our group and others have demonstrated that metal decoration on anatase TiO_2 nanoparticles and nanotubes has a significant effect in converting them into visible light active photocatalysts.[20-25] Similarly, transition metal or nonmetal doping within the TiO_2 lattice is also a popular strategy for increasing its visible light absorption.[10,26-28] Among different doping strategies, nitrogen doping has been the most popular and effective method, with more recent studies showing the effect of more than one nonmetal codoping in TiO_2 lattice towards enhanced visible light absorption and thereby the photocatalytic activity.[10,26,27] To this end, strategies involving doping of TiO_2 lattice with more than two non-metals simultaneously are rather rare.[10,13,26,27,29]

Moreover, in most of the studies that focus on nonmetal or metal codoping, the control over the morphology of TiO_2 nanoparticles formed during the codoping process remains elusive and challenging. To this end, our group and others have shown that the use of an IL during the synthesis of inorganic materials allows the IL to form an organic template, which provides a control over nucleation process that in turn, assists in controlling the morphology of the targeted nanomaterial.[5-8] Therefore, we envisaged that by replacing conventional aqueous and organic solvents typically used for TiO_2 nanoparticles synthesis with an IL in the presence of a mild hydrolysing agent might significantly influence the reaction outcomes. The current study discusses these findings by demonstrating the facile synthesis of multiple nonmetals codoped rutile titania nanorods through using [BMIM][BF_4] as a designer IL solvent, wherein three nonmetals viz. nitrogen, carbon and fluorine are observed to simultaneously codope the TiO_2 lattice. Considering that non-metal doping can favourably influence the band edge as well as the charge recombination

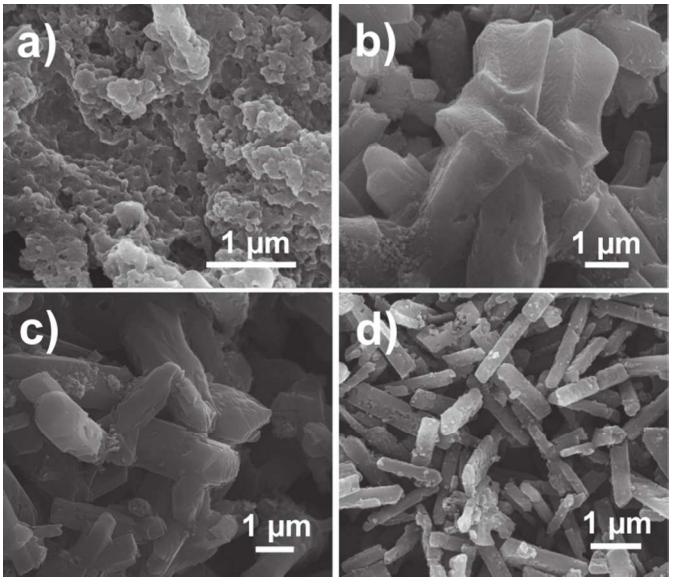

Fig. 1 SEM images of titania nanostructures synthesized in [BMIM][BF_4] IL by hydrolysing 1 mM $TiCl_3$ using different concentrations of ammonia (a) 0.56% , (b) 0.28%, (c) 0.14% and (d) 0.06%.

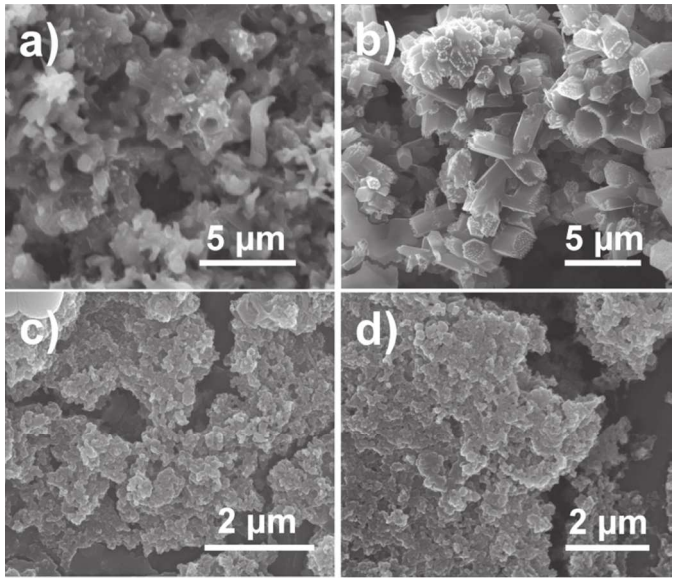

Fig. 2 SEM images of titania nanostructures synthesized in [BMIM][BF_4] by hydrolysing 1 mM $TiCl_3$ using 0.06% ammonia and varying water concentration (a) 10 µL , (b) 30 µL, (c) 40 µL and (d) 50 µL.

process in semiconductors during photoexcitation, these NCF-codoped rutile TiO_2 nanorods could remarkably enhance the UV and visible light photocatalytic degradation of a Congo red (CR), a model azo dye, in comparison to commercial Degussa P25 TiO_2 nanoparticles.

In a typical synthesis, 1 mM titanium trichloride ($TiCl_3$) was independently exposed to decreasing concentration of liquid ammonia in the presence of IL [BMIM][BF_4] at 25 ± 0.1 °C at 1,200 rpm for 24 h (ESI, see Methods for details). Similarly, in a control experiment, liquid ammonia was replaced with water. In IL, all solutions containing $TiCl_3$ and ammonia became turbid, suggesting the hydrolysis of $TiCl_3$ precursor by ammonia. However, control experiments did not show turbidity thereby negating the possibility of water-mediated hydrolysis of $TiCl_3$ in IL. Importantly, the water content in all these reactions was kept constant to understand the role of water during the formation of the nanostructures. The reaction products were centrifuged and washed several times in acetonitrile (to remove viscous IL) and the obtained precipitates were characterised.

Fig. 1 shows the representative SEM images of titania particles obtained in IL while employing the final ammonia concentrations of 0.56% (a), 0.28% (b), 0.14% (c) and 0.06% (d), respectively. Additional lower magnification SEM images are illustrated in Fig. S1 (ESI). With decreasing concentrations of hydrolysing agent, a significant control over the morphology of titania particles can be seen. At high concentrations of ammonia, the as-synthesised particles were found to be fused quasi-spheres (Fig. 1a). Lowering the concentration of ammonia to 0.28% and 0.14% allowed a control over the morphology of the particles leading to fused rod-like structures (Fig. 1b and 1c). Upon further lowering the concentration of ammonia, well defined rod-shaped nanoparticles of 2-5 µm in length and several hundred nanometers in thickness were observed (Fig. 1d). It is although interesting to observe the control over rod-like morphology of titania in [BMIM][BF_4], it is not surprising considering that ILs have been previously shown to have significant influence over the morphology of targeted nanomaterials.[2,5,7-9,30] In fact, in one of our previous studies, wherein we employed cationic amino acids (lysine, arginine and histidine) for hydrolysing a silica precursor in ILs, a similar amino acid concentration-dependent trend influencing the overall morphology of silica nanostructures was observed.[7] Such control over the morphology of nanomaterials synthesized in ILs has been attributed to the ability of ILs to promote a diffusion limited aggregation process that can lead to the stabilization of different nanostructured morphologies.[7,30,31]

It is well recognised that water molecules can form channels within the complex matrices of viscous ILs and these channels can act as reaction sites leading to interesting morphologies.[4,5,31,32] To further understand the role of water during the formation of nanorods, we employed different concentrations of water during hydrolysis while keeping the concentration of ammonia and the precursor constant. Particular care was taken to keep the concentration of ammonia at 0.06 % as stable nanorods were obtained at this concentration. However, changing the water concentration from the original 20 µL per mL of reaction to 10, 30, 40 or 50 µL per mL resulted in loss of rod-like morphology (**Fig. 2**). It is evident that even a small change in the concentration of water (±10 µL) disrupts the stable rod-like morphology. Although the morphology is disrupted, at 10 (Fig. 2a) or 30 µL per mL (Fig. 2b) water concentration, the nanostructures still exhibit a rod-like morphology, albeit found fused. Increasing the water concentration beyond 30 µL per mL (Fig. 2c and 2d) results in a complete loss of rod-like morphology leading to fused quasi-spherical structures, similar to that observed at high concentrations of ammonia. This small change in the water concentration leading to morphological change points us to the important role of water during the hydrolysis process. As outlined in previous studies, the formation of channels by water may influence the formation of rod-like morphology during the hydrolysis process.

To understand the influence of IL on composition of titania nanorods, vibrational spectroscopic analysis was performed. The FTIR spectrum of the nanorods exhibited characteristic lattice vibrations of TiO_2 below 850 cm^{-1} (ESI, Fig. S2).[33] Additionally, peaks corresponding to [BMIM][BF_4] were

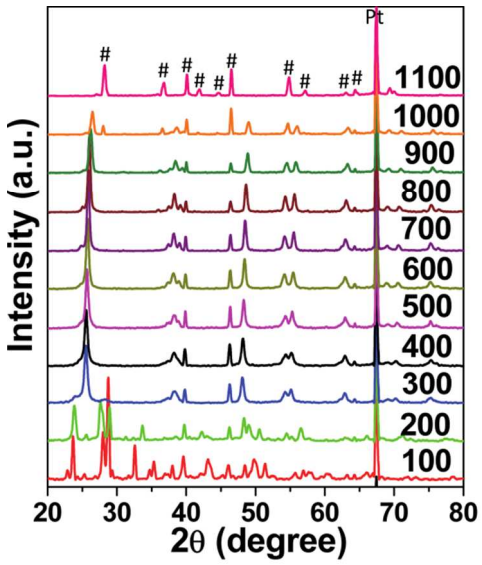

Fig. 3 HT-XRD of titania nanostructures synthesized in [BMIM][BF_4] by hydrolyzing 1 mM $TiCl_3$ using 0.06% ammonia. (#) correspond to the diffraction peaks arising from rutile TiO_2.

observed, suggesting the role of IL in controlling the nanorod morphology. FTIR suggested that the rod-like morphology may be driven due to the π-π stacking of the imidazolium rings of $[BMIM]^+$ cations in IL, as evident from the change in the aromatic stretching mode between 3200-3000 cm^{-1} (grey region marked in Fig. S2).[34] In comparison to pristine IL, substantial broadening and a shift of these vibrational modes were observed towards lower wavenumbers in nanorods, which are due to the decrease in the electron density of the ring C-H bonds. The packing of the positively charged imidazolium rings is also evident from the peak broadening observed ca. 2950-2850 cm^{-1}, which arises due to the packing of the butyl group of $[BMIM]^+$ cations.[34] These observations suggest the incorporation of IL [BMIM][BF_4] in as-synthesized titania and its potential role in influencing the nanorod-like morphology of titania structures.

To ascertain the nature of the as-synthesised material, XRD analysis was performed on the well-formed nanorods obtained at the lowest concentration of ammonia solution. The as-synthesised material showed a polycrystalline nature (ESI, Fig. S3); however the diffraction peaks could not be matched with any known indexed phase of titania or the well-reported hydrogen or ammonium titanate. The efforts to perform the Rietveld refinement on this XRD pattern also did not provide any conclusive information. Nevertheless, some of these peaks matched with brookite phase but the lack of a clear indexation could not confirm the material. Therefore, to obtain phase pure TiO_2 nanorods and to understand the phase transformation of the as-synthesised nanorods, high temperature XRD (HT-XRD) was performed while gradually heating up the material up to 1100 °C. **Fig. 3** shows the phase transformation of the nanorods at different temperatures. It is evident that the as-synthesised polycrystalline material undergoes several changes in its structure up to 300 °C, following which a stabilisation of the XRD patterns is observed. Although most of the peaks observed at this temperature match with brookite TiO_2, some of these peaks also overlap with the rutile phase.[17,35] The material undergoes subtle changes until 900 °C, following which a phase transformation between 1000–1100 °C leading to the stabilisation of rutile phase (JCPDS 21-1272), is observed. This

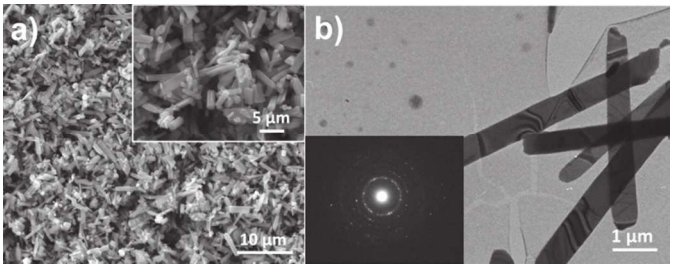

Fig. 4 (a) SEM and (b) TEM images of phase pure rutile TiO_2 nanorods. Inset in (b) correspond to selected area diffraction pattern from nanorods shown in the main image.

phase pure rutile TiO_2 was further characterised using SEM and TEM (**Fig. 4**), which showed that while these structures retained their original rod-like morphology, the dimensions of rutile nanorods changed to 5-20 µm in length with thickness averaging 200-500 nm. The selected area electron diffraction (SAED) pattern from these structures further confirmed that the nanorods were indeed consisted of phase pure rutile TiO_2.

FTIR analysis provides an understanding towards the role of [BMIM][BF_4] in synthesising nanorods, however it is incapable of providing information on the possibility of rutile TiO_2 codoping with nonmetals such as N, C, F and B that are present in the original IL structure. It is well known that TiO_2 lattice can be codoped with metals and nonmetals during calcination in a controlled oxygen rich environment. To identify the possible dopants in the rutile nanorods, their surface chemical analysis was performed using x-ray photoemission spectroscopy (XPS), which is a highly surface sensitive technique. **Fig. 5** shows C 1s, N 1s, O 1s, Ti 2p and F 2p core level XPS spectra arising from rutile nanorods. All XPS spectra were background corrected using Shirley algorithm, and their respective binding energies (BEs) were aligned to the C 1s BE of 285 eV.[36] Further, a Gaussian-Lorentzian function was applied to fit the core level components of individual spectrum to understand their mode of doping either in the TiO_2 lattice or presence on the TiO_2 surface. The C 1s core level could be deconvoluted into three components with the predominant BE component at 285 eV arising from adventitious carbon; and two

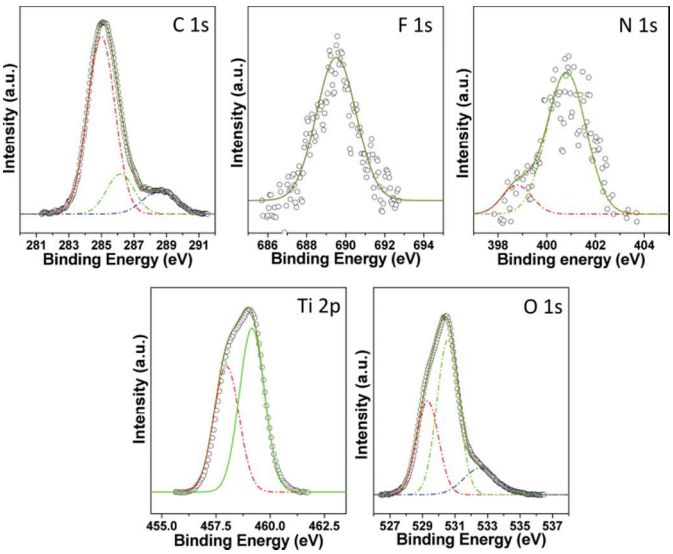

Fig. 5 XPS spectra showing C 1s, O 1s, Ti 2p, F 1s and N 1s core levels from phase pure NCF-codoped rutile TiO_2 nanorods.

lower BE components at ca. 286.2 eV and 288.6 eV, which correspond to C-O species.[37] The presence of C-O species suggests that the carbon atom is not directly bound to the Ti; however it is bound via Ti-O-C linkage, which corroborates well with similar signatures observed for C-doped TiO_2.[37] Although the 288.6 eV BE component shows a shift of 0.3 eV towards higher BE over that previously reported for C-doped TiO_2, this shift is expected given the potential presence of highly electronegative F^- atoms from $[BF4]^-$ anion of IL. Similarly, the N 1s core level could be deconvoluted into two major components with BEs ca. 398.8 eV and 400.7 eV. The lower N 1s BE component is due to the N atoms incorporated in O−Ti−N linkages, while the higher BE peak is due to electronegative O atoms directly attached to N atoms in Ti−O−N or Ti−N−O linkages. The absence of low BE peak at 396 eV establishes the absence of a potential TiN species.[38,39] With respect to fluorine, the F 1s core level shows only one component at ca. 689.2 eV. This peak arises mainly due to the doping of F within the TiO_2 lattice, and not due to the replacement of surface hydroxyl groups of TiO_2 with F^- ions.[40] In previous studies, it has been shown that the incorporation of F into TiO_2 lattice may occur through nucleophilic substitution of O atoms during hydrolysis of a titania precursor in the presence of F^- ions. Since the atomic radii of F^- and O^{2-} are similar, the thermal energy during the heating of a titanate material can trigger such substitutions within the lattice structure.[40] No signature corresponding to B 1s or Cl 2p core level was detected in XPS, suggesting that boron or chlorine did not dope into the lattice of rutile TiO_2 nanorods during the heating process.

Further, the Ti 2p core level XPS spectrum could be fitted into two spin-orbit pairs (spin-orbit splitting of 5.3 eV) with $2p_{3/2}$ BEs of 458.3 and 459.1 eV. These BEs are lower than those expected from non-doped TiO_2 (458.7 eV),[38] clearly indicating that nonmetals are effectively doped into TiO_2 lattice through substitution of O atoms. Since C, N, O and F show increasing electronegativities, it is expected that substitutional replacement of O in O–Ti–O structure of TiO_2 lattice with F will cause a higher BE shift in Ti 2p core level, while such replacements with N and C will result in shifts toward lower BEs. Notably, out of the two Ti 2p core level BEs observed in this study, the lower BE component at 458.3 eV lies lower than that of non-doped TiO_2 (458.7 eV)[38] and in between C-doped[37] (458.5) and N-doped[38,39] (458.2) TiO_2. This provides clear evidence that rutile TiO_2 nanorods are codoped with carbon and nitrogen. Similarly, the higher BE component at 459.1 eV observed in this study lies in between non-doped (458.7)[38] and F-doped[40,41] TiO_2 (459.5), providing further evidence that rutile TiO_2 nanorods are also codoped with F atoms. These observed Ti 2p core level BEs also support the information obtained from N 1s, C 1s and F 1s core levels, which also indicate the partial substitution of O in TiO_2 lattices by N, C and F to yield NCF-codoped rutile TiO_2 nanorods in this study. Further evidence of NCF codoping into TiO_2 lattice is evident from O 1s core level that could be deconvoluted into three BEs components at ca. 529.5 eV, 530.7 eV and 532.6 eV. The major BE component at 530.7 eV is due to the presence of O-Ti-O bonds, while the peaks observed at lower and higher BEs are due to the presence of N/C,[37-39] and F,[40, 41] respectively in TiO_2 lattice.

The detailed XPS analysis provides convincing evidence in favour of partial substitutional codoping of N, C and F in the lattice of rutile TiO_2 nanorods. Although nonmetal doping of TiO_2 is well established, most of the previous efforts to create nonmetal-doped TiO_2 have resulted in doping with a single or

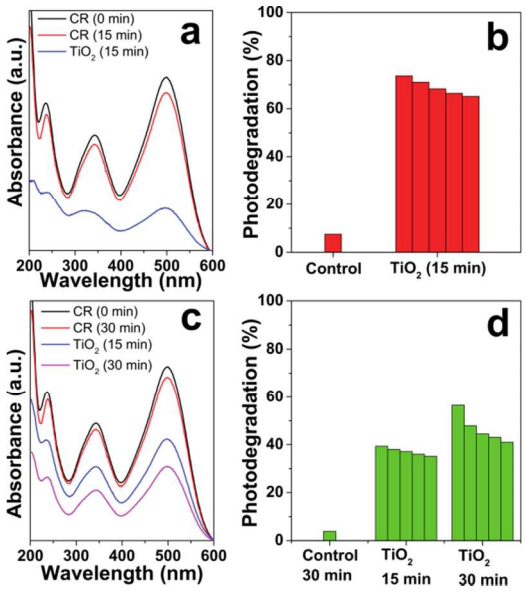

Fig. 6 UV-visible absorbance spectra of the Congo red (CR) upon exposure to NCF-codoped rutile TiO_2 nanorods for (a) 15 min under UV light conditions and (c) 15 and 30 min under visible light conditions. Percentage photodegradation of CR expressed as reduction in the intensity of A_{500} on its exposure to NCF-codoped rutile TiO_2 nanorods in the presence of (b) 253 nm UV light for 15 min and (d) 575 nm visible light for 15 and 30 min. The five bars within each of the catalyst indicate the activity of photocatalyst during reusability for five cycles.

two nonmetals.[10] This nonmetal doping of TiO_2 is observed to shift its band edge in the visible region, thereby allowing TiO_2 to act as a visible light photocatalyst. Therefore, the NCF-codoped rutile TiO_2 reported in this study may have significant influence in promoting visible light-induced photocatalytic reactions. Moreover, the recombination of charge carriers (electrons and holes) during photoexcitation of a semiconductor such as TiO_2 is one of the primary concerns that hampers their ability to perform efficient photocatalysis.[29] During photoexcitation of the materials by incident photons, electrons jump from valence band (VB) across the band gap toward the conduction band (CB); however, these newly generated electron-hole pairs tend to recombine again.[29] The doping of nonmetals within a semiconductor lattice can allow the control of band gap energy levels by narrowing it thereby creating an acceptor level above the VB maximum.[10] This may therefore result in significant improvement in the photocatalytic performance of such doped semiconducting materials. Therefore, to investigate the influence of NCF-codoping in rutile TiO_2 nanorods, their photocatalytic activity toward the photodegradation of a model azo dye Congo red (CR) was evaluated in the presence of both UV (253 nm) and visible light (575 nm) excitation sources.

It is well-known that the exposure of UV light to CR dye in the absence of any catalyst can promote its breakdown to some extent, which can be monitored by measuring the change in the characteristic absorbance at ca. 500 nm using UV-visible spectroscopy (**Fig. 6**). On exposure to UV light for 15 min, this accounted for 8% CR degradation in the absence of a catalyst. In contrast, in the presence of NCF-codoped rutile TiO_2 nanorods, 73% dye degradation was observed. When these nanorods were separated from the reaction solution, post-reaction by centrifugation and reused for CR degradation, they showed comparable activities for at least five repeated cycles. The dye photodegradation ability of these nanorods over

multiple cycles also suggests that the observed photoactivity is in fact due to the photoactivity of rutile nanorods, and not due to nonspecific adsorption of dye molecules onto nanorods surface. Further, in contrast to UV excitation experiments, the visible light experiments were performed for longer time periods as the degradation of dye is relatively slower in the latter. In visible light, the control experiment showed only 6% photodegradation of CR over 30 min exposure while NCF-codoped TiO_2 caused 56% dye degradation. In contrast to the 73% photodegradation observed under UV-light within 15 min, visible light exposure for 15 min led to 40% dye degradation. When activity of NCF-codoped TiO_2 was compared with equivalent weight amounts of commercial Degussa P-25 TiO_2 nanoparticles, it led to only 18% CR photodegradation in UV light (15 min) and 9% CR photodegradation in visible light (30 min). Since catalytic activity of a nanomaterial is strongly influenced by its overall surface area, the BET surface area of commercial Degussa P-25 TiO_2 nanoparticles and NCF-codoped TiO_2 nanorods prepared in this study were compared. While commercial TiO_2 nanoparticles showed a surface area of ca. 134 m^2/g, the surface area of NCF-codoped rutile TiO_2 nanorods was found to be ca. 6.87 m^2/g. Interestingly, although the surface area of the commercial TiO_2 was almost 20 times higher than that of the NCF-codoped TiO_2, the latter showed 4 times and 4.4 times higher photocatalytic activity under UV and visible irradiation conditions, respectively, over that of the former. This comparison clearly highlights the importance of multiple nonmetals (NCF) codoping in rutile TiO_2 nanorods for allowing it to behave as an outstanding photocatalyst both under visible and UV-light excitation conditions.

In summary, this study demonstrates a facile route to synthesise multiple nonmetal NCF-codoped rutile TiO_2 nanorods that not only display enhanced photocatalytic performance in UV-light, but also allow a significant level of visible light photocatalytic activity. The use of IL [BMIM][BF_4] as a solvent for TiO_2 synthesis provides a control over nanoparticle morphology to form nanorods via providing water channels within IL that act as soft templates during hydrolysis of titania precursor. Moreover, the presence of different nonmetals in the IL solvent offers a unique strategy to dope these nonmetals (N, C and F) into TiO_2 lattice via heating of as-synthesized material. This study therefore underlines the importance of ILs as interesting solvents to control mineral morphology and composition. It is likely that in future, other nonmetals may also be doped in the lattice of TiO_2 and other oxides through careful choice of ILs during metal oxide synthesis. Furthermore, the multiple nonmetals-codoped TiO_2 nanorods reported in this study may provide a significant edge over commercially available nanoparticulate TiO_2, both for UV and visible light-activated photocatalysis.

Acknowledgements

V. Bansal thanks the Australian Research Council for a Future Fellowship (FT140101285) and research funding through the Discovery (DP0988099, DP110105125) and Linkage (LP100200859) grant schemes. V. Bansal also acknowledges the generous support of the Ian Potter Foundation for establishing a multimode spectroscopy facility and an Ian Potter NanoBioSensing Facility at RMIT University. Authors acknowledge the support from the RMIT Microscopy and Microanalysis Facility (RMMF) for technical assistance and providing access to characterisation facilities.

Notes and references

[a]Ian Potter NanoBioSensing Facility, NanoBiotechnology Research Laboratory, School of Applied Sciences, RMIT University, GPO Box 2476 V, Melbourne VIC 3001, Australia.
*Corresponding author: Email- vipul.bansal@rmit.edu.au; Tel: +61 399252121, Fax: +61 3 99253747.

Electronic Supplementary Information (ESI) available: [Methods, SEM images, FTIR spectra and XRD pattern]. See DOI: 10.1039/b000000x/

1. Armand, M.; Endres, F.; MacFarlane, D. R.; Ohno, H.; Scrosati, B. *Nat. Mater.* **2009,** 8, (8), 621-629.
2. Ryu, Hyung J.; Sanchez, L.; Keul, Heidrun A.; Raj, A.; Bockstaller, Michael R. *Angew. Chem. Int. Ed.* **2008,** 47, (40), 7639-7643.
3. Mulet, X.; Kennedy, D. F.; Greaves, T. L.; Waddington, L. J.; Hawley, A.; Kirby, N.; Drummond, C. J. *J. Phys. Chem. Lett.* **2010,** 1, (18), 2651-2654.
4. Greaves, T. L.; Drummond, C. J. *Chem. Soc. Rev.* **2013,** 42, (3), 1096-1120.
5. Greaves, T. L.; Drummond, C. J. *Chem. Soc. Rev.* **2008,** 37, (8), 1709-1726.
6. Soni, S. K.; Ramanathan, R.; Coloe, P. J.; Bansal, V.; Bhargava, S. K. *Langmuir* **2010,** 26, (20), 16020-16024.
7. Ramanathan, R.; Campbell, J. L.; Soni, S. K.; Bhargava, S. K.; Bansal, V. *PLoS ONE* **2011,** 6, (3), e17707.
8. Ma, Z.; Yu, J.; Dai, S. *Adv. Mat.* **2010,** 22, (2), 261-285.
9. Pearson, A., O'Mullane, A. P.; Bhargava, S. K.; Bansal, V. *Langmuir* **2013**, 29 (1), 8-12.
10. Chen, X.; Mao, S. S. *Chem. Rev.* **2007,** 107, (7), 2891-2959.
11. Bansal, V.; Bharde, A.; Ramanathan, R.; Bhargava, S. K. *Adv. Colloid Inter. Sci.* **2012,** 179, 150-168.
12. Bansal, V.; Ramanathan, R.; Bhargava, S. K. *Aust. J. Chem.* **2011,** 64, (3), 279-293.
13. Daghrir, R.; Drogui, P.; Robert, D. *Ind. Eng. Chem. Res.* **2013,** 52, (10), 3581-3599.
14. Schwartzenberg, K. C.; Gray, K. A. *Catal. Sci. Technol.* **2012,** 2, (8), 1617-1624.
15. Zhang, R.; Elzatahry, A. A.; Al-Deyab, S. S.; Zhao, D. *Nano Today* **2012,** 7, (4), 344-366.
16. Addamo, M.; Bellardita, M.; Di Paola, A.; Palmisano, L. *Chem. Commun.* **2006**, (47), 4943-4945.
17. Dambournet, D.; Belharouak, I.; Amine, K. *Chem. Mater.* **2009,** 22, (3), 1173-1179.
18. Li, J.-G.; Ishigaki, T.; Sun, X. *J. Phys. Chem. C.* **2007,** 111, (13), 4969-4976.
19. Mohamed, A. E. R.; Rohani, S. *Energy Environ. Sci.* **2011,** 4, (4), 1065-1086.
20. Pearson, A.; Zheng, H.; Kalantar-zadeh, K.; Bhargava, S. K.; Bansal, V. *Langmuir* **2012,** 28, (40), 14470-14475.
21. Pearson, A.; Bhosale, S.; Bhargava, S. K.; Bansal, V. *ACS Appl. Mater. Inter.* **2013,** 5, (15), 7007-7013.
22. Yang, L.; He, D.; Cai, Q.; Grimes, C. A. *J. Phys. Chem. C.* **2007,** 111, (23), 8214-8217.
23. Kamat, P. V. *J. Phys. Chem. B.* **2002,** 106, (32), 7729-7744.
24. Subramanian, V.; Wolf, E.; Kamat, P. V. *J. Phys. Chem. B.* **2001,** 105, (46), 11439-11446.
25. Subramanian, V.; Wolf, E. E.; Kamat, P. V. *Langmuir* **2002,** 19, (2), 469-474.
26. Zaleska, A. *Recent Pat. Eng.* **2008,** 2, (3), 157-164.
27. Dozzi, M. V.; Selli, E. *J. Photochem. Photobiol. C.* **2013,** 14, 13-28.
28. Liu, G.; Wang, X.; Wang, L.; Chen, Z.; Li, F.; Lu, G. Q.; Cheng, H.-M. *J. Colloid Inter. Sci.* **2009,** 334, (2), 171-175.
29. Linsebigler, A. L.; Lu, G.; Yates, J. T. *Chem. Rev.* **1995,** 95, (3), 735-758.
30. Pearson, A.; O'Mullane, A. P.; Bansal, V.; Bhargava, S. K. *Chem. Commun.* **2010,** 46, (5), 731-733.
31. Castner Jr, E. W.; Margulis, C. J.; Maroncelli, M.; Wishart, J. F. *Annu. Rev. Phys. Chem.* **2011,** 62, 85-105.
32. Greaves, T. L.; Drummond, C. J. *Chem. Rev.* **2007,** 108, (1), 206-237.
33. Nakamura, R.; Imanishi, A.; Murakoshi, K.; Nakato, Y. *J. Am. Chem. Soc.* **2003,** 125, (24), 7443-7450.

34. Zhou, Y.; Schattka, J. H.; Antonietti, M. *Nano Lett.* **2004,** 4, (3), 477-481.
35. Li, J.-G.; Ishigaki, T. *Acta Biomater.* **2004,** 52, (17), 5143-5150.
36. Bansal, V.; Rautaray, D.; Bharde, A.; Ahire, K.; Sanyal, A.; Ahmad, A.; Sastry, M. *J. Mater. Chem.* **2005,** 15, (26), 2583-2589.
37. Ren, W.; Ai, Z.; Jia, F.; Zhang, L.; Fan, X.; Zou, Z. *Appl. Cat. B.* **2007,** 69, (3-4), 138-144.
38. Jagadale, T. C.; Takale, S. P.; Sonawane, R. S.; Joshi, H. M.; Patil, S. I.; Kale, B. B.; Ogale, S. B. *J. Phys. Chem. C.* **2008,** 112, (37), 14595-14602.
39. Zhang, Z.; Wang, X.; Long, J.; Gu, Q.; Ding, Z.; Fu, X. *J. Catal.* **2010,** 276, (2), 201-214.
40. Yu, J. C.; Yu; Ho; Jiang; Zhang, Y. *Chem. Mater.* **2002,** 14, (9), 3808-3816.
41. Dozzi, M. V.; D'Andrea, C.; Ohtani, B.; Valentini, G.; Selli, E. *J. Phys. Chem. C.* **2013,** 117, (48), 25586-25595.

